The Effects of I/Q Imbalance and Complex Filter Mismatch on GPS/Galileo System

Pei-Hsueh Lee, *National Taiwan University*
Ho-Ching Chao, *National Taiwan University*
Wei-Lung Mao, *National Formosa University*
Hen-Wai Tsao, *National Taiwan University*
Fan-Ren Chang, *National Taiwan University*

BIOGRAPHY

Pei-Hsueh Lee was born in Taiwan, R.O.C., in 1981. He received the B.S. degree in communication engineering from National Chiao Tung University, Taiwan in 2003, and the M.S. degree in communication engineering from National Taiwan University, Taiwan in 2005. He is currently working for his Ph.D. degree in National Taiwan University, Taiwan. His research interests are satellite navigation systems, wireless communications, and digital signal processing.

Ho-Ching Chao was born in Taiwan, R.O.C. in 1983. He received the B.S. degree in electrical engineering from National Chung Hsing University in 2005, and the M.S. degree in communication engineering from National Taiwan University in 2007. He is currently serving in the army for his mandatory military service.

Wei-Lung Mao was born in Taiwan, R.O.C. in 1972. He received the B.S. degree in electrical engineering from National Taiwan University of Science and Technology in 1994, and the M.S. and Ph.D. degrees in electrical engineering from National Taiwan University in 1996 and 2004, respectively. He is now an assistant professor in the Department of Electronic Engineering, National Formosa University. His research interests are satellite navigation systems, adaptive signal processing, neural networks and communication electronics.

Hen-Wai Tsao received the B.S., M.S., and Ph.D. degrees in electrical engineering from National Taiwan University, Taipei, Taiwan, R.O.C. in 1975, 1978, and 1990, respectively. He joined the faculty of the Department of Electrical Engineering, National Taiwan University in 1978 and became a professor in 1991. His main research interests are broadband communication system, communication electronics, and electronic instrumentation. He is a member of IEEE.

Fan-Ren Chang was born in Taiwan, on October 6, 1949. He received the B.S. and M.S. degrees from National Chiao Tung University, Taiwan, in 1972 and 1974 respectively, the Ph.D. degree from University of Houston, Texas, in 1985, all in electrical engineering. From 1976 to 1981, he was an assistant researcher of Chung Shan Institute of Science and Technology. He worked for missile and fire control system projects. He joined the Department of Electrical Engineering, National Taiwan University in 1985 as an associate professor. Since 1990, he has been a professor at the same department. He was the visiting professor of EE Department of Stanford University from October 2002 to February 2003. His research interests include linear multivariable systems, generalized systems, numerical algorithms, and satellite navigation systems.

ABSTRACT

As global navigation satellite systems thrive recently, there are urgent need and demand for integrated modeling of analog circuits such that the system performance can be predetermined. This paper analyzes the errors of mixers and complex filters within the analog front-end, and describes their effects of nonidealities on image rejection, which is an important indicator for the signal quality. It has shown the design considerations for complex filters must take account of not only the out-of-band attenuation but also the components instabilities per se as well. Besides, unavoidable I/Q imbalance of analog mixers exacerbates the situation, hence it is useful to acquire the design tolerance in advance for both mixers and complex filters.

INTRODUCTION

Galileo global navigation satellite system is a worldwide program launched by the European Union (EU) and the European Space Agency (ESA), providing complementarity with the existing GPS, and it will be Europe's own navigation system, offering a highly accurate, guaranteed global positioning service. Satellite navigation is an advanced technology. It is based on the signals emitted from satellites to indicate the time extremely precisely such that any individual can determine his position or the location of any moving or stationary object. Galileo is based on a constellation of 30 satellites with ground controlling stations and will be inter-operable with the omnipresent GPS. For instance, Galileo E1B/E1C shares common central frequency with that of GPS L1 such that users

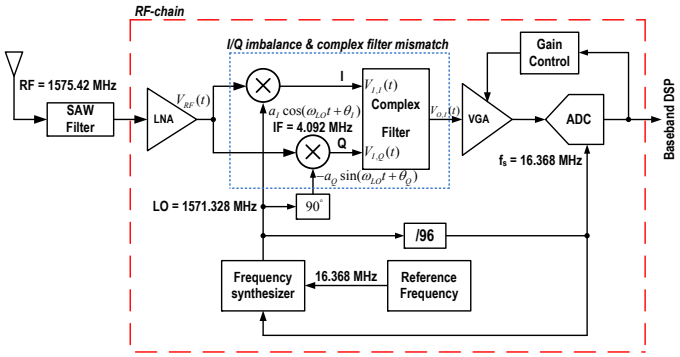

Fig. 1. A typical image-rejected low-IF GPS/Galileo receiver.

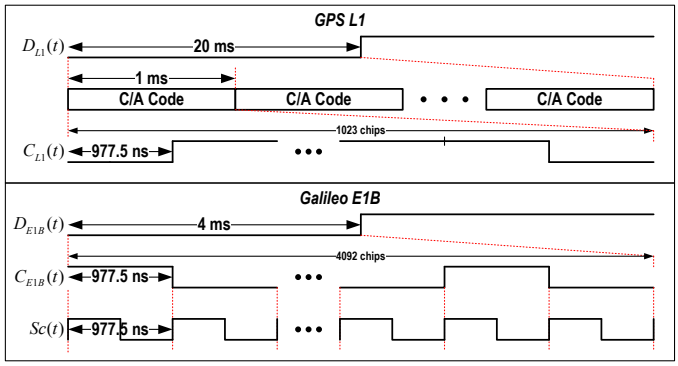

Fig. 2. GPS/Galileo signal timing.

will be capable to determine the position in the same receiver assisted by any of these satellites in any combination.

Comparing different types of receiver architectures, a low-IF (intermediate frequency) receiver brings a compromised solution for GPS and Galileo commercial products [1], [2], [3]. It provides high level of integration for cost reduction while avoiding the problem of D.C. offset that usually degrades the system performance in a zero-IF receiver. However, the image signal situated at twice the IF frequency from the desired signal will jam into the signal band after being down-converted to the intermediate frequency. Even in the absence of interfering signals lying in the image band, ubiquitous thermal noise can still ruin the carrier to noise ratio by a factor of 3 dB that is critical particularly in noisy environments, and could be worse when strong interference exists.

Fig. 1 illustrates the structure of a typical low-IF receiver where the carrier frequency of the received signal from the antenna is 1575.42 MHz. The received signal is first selected by the SAW filter and then amplified by the LNA. Because the IF is 4.092 MHz, the amplified signal has to be mixed with a LO of 1571.328 MHz. Therefore, a temperature compensated crystal oscillator (TCXO) with the reference frequency of 16.368 MHz and a divider with the divide ratio 96 are used to generate the desired single tone. Once the signal has been down-converted to the IF, a complex filter not only provides channel selection but also enhances resistance to the image is commonly adopted. Since it requires its two inputs to be quadrature, two mixers as shown in Fig. 1 are needed. The signal level after complex filtering is adjusted by a variable gain amplifier (VGA) and digitized by a 2-bit ADC.

In this paper, after briefly reviewing the fundamentals of modulation used by GPS and Galileo, the mixer imbalance model is formulated in subsequent section. Following the discussion of mixers imbalance is the modeling of complex filters where we demonstrate the design procedures for Gm-C type complex filters and clarify the filter mismatch and mixer imbalance can be modeled together in terms of transfer functions. Final sections are the simulation results and the conclusions that conclude this paper.

GPS/GALILEO SIGNALING ON L1 BAND

Both GPS and Galileo exploit direct sequence spread spectrum (DSSS) technique to transmit their ranging signals. The nature of DSSS makes itself a good candidate for ranging applications. By observing the received code phase after Doppler wipe-off, one can determine the distance between the transmitting satellite and the user. By decoding the ranging message in the received signal, the position of the time when the satellite started to transmit the signal can be resolved. With both knowledge, the location of the receiving antenna can be fixed.

Galileo satellites utilize binary offset carrier (BOC) modulation to convey their ranging messages. The BOC modulation differs from BPSK used by GPS in that it imposes an additional square-shaped subcarrier to the transmitting signal. In literature [4], a BOC(m,n) representation specifies the subcarrier frequency $f_{sc} = mf_0$ and the chip rate $f_c = nf_0$ where the normalized frequency $f_0 = 1.023$ MHz. For example, a BOC(1,1) signal has a subcarrier frequency of 1.023 MHz and a code chip rate of 1.023 Mcps. Both signals can be expressed mathematically as

$$s_{L1}(t) = D_{L1}(t)C_{L1}(t) \tag{1}$$

$$s_{E1B}(t) = D_{E1B}(t)C_{E1B}(t)Sc(t)\,, \tag{2}$$

where $D_{L1}(t)$ and $D_{E1B}(t)$ are the navigation data of GPS L1 and Galileo E1B, respectively. For simplicity, only the data channel, E1B, is considered. $C_{L1}(t)$ is the coarse/acquisition (C/A) spreading code for GPS L1 while $C_{E1B}(t)$ is the ranging code for Galileo E1B, and

$$Sc(t) = \mathrm{sign}\big(\sin(2\pi f_{sc}t)\big)\,, \tag{3}$$

is the subcarrier. All of these binary signals are encoded using rectangular pulse amplitude modulation with the non-return-to-zero code.

The symbol rate of GPS L1 is 50 sps, that is, each binary symbol takes 20 ms to transmit. There are totally 20 identical C/A code periods within one data symbol, so each C/A code period is 1 ms. Since one C/A code contains 1,023 chips, the duration of each code chip is roughly about 977.5 ns. In terms of Galileo E1B, each symbol duration is 4 ms at a symbol rate of 250 sps. Since there are 4,092 chips within one E1B spreading code, the code chip duration is the same as that of GPS.

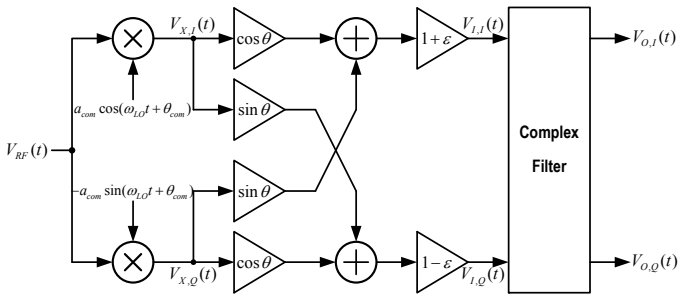

Fig. 3. Mixer imbalance model.

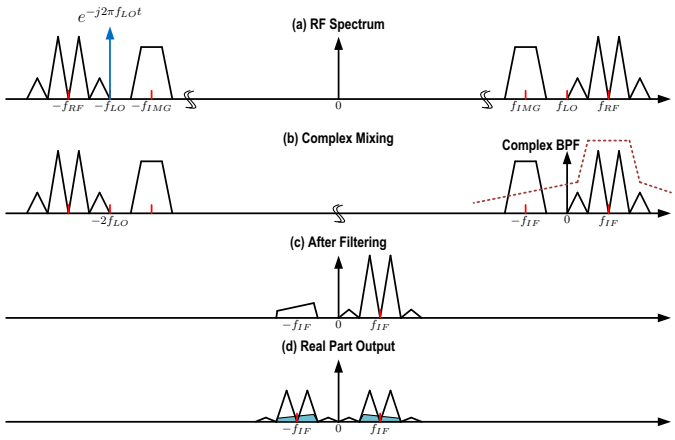

Fig. 4. Role of a complex bandpass filter in the front-end chain.

As shown in Fig. 2, it can be seen the most apparent difference in signaling for GPS and Galileo is the subcarrier modulation. For GPS, in order to accommodate the main lobe of its spreading signal, the front-end filtering should have a passband bandwidth larger than 2.046 MHz. Due to the subcarrier modulation of Galileo, the main lobe is translated to bilateral sides with respect to the carrier frequency of the signal. The amount of translation is determined by the subcarrier frequency that is 1.023 MHz for BOC(1,1). In consequence, the filtering bandwidth for a GPS/Galileo receiver will have to be at least greater than 4.092 MHz so as to receive the two-side lobes.

MODELING OF I/Q IMBALANCE IN MIXERS

In order to model the imbalance of amplitude and phase between in-phase and quadrature-phase signals generated from the frequency synthesizer, each amplitude and phase component is decomposed as the combination of a common-mode and a differential signal. According to Fig. 1, define the common-mode amplitude a_{com} and differential amplitude a_{dif} between I/Q as

$$a_{com} = \frac{a_I + a_Q}{2} \tag{4}$$

$$a_{dif} = a_I - a_Q\,, \tag{5}$$

where a_I and a_Q are the amplitude components of I- and Q-path, respectively, and the common-mode phase θ_{com} and differential phase θ_{dif} between I/Q are defined as

$$\theta_{com} = \frac{\theta_I + \theta_Q}{2} \tag{6}$$

$$\theta_{dif} = \theta_I - \theta_Q\,, \tag{7}$$

where θ_I and θ_Q are the phase components of I- and Q-path, respectively. When the mixers are perfectly balanced, one can expect $a_I = a_Q$ and $|\theta_I - \theta_Q| = \pi/2$, that is, besides amplitude components of I/Q are identical, phase difference between I/Q is exact $\pi/2$.

After rewriting the amplitude and phase component of I as

$$\begin{aligned} a_I &= (a_{com} + a_{dif}/2) = a_{com}(1 + \frac{a_{dif}/2}{a_{com}}) \\ &= a_{com}(1+\epsilon) \\ \theta_I &= \theta_{com} + \theta_{dif}/2 \\ &= \theta_{com} + \theta\,, \end{aligned} \tag{8}$$

where $\epsilon \triangleq \frac{a_{dif}/2}{a_{com}}$ is the amplitude mismatch and $\theta \triangleq \theta_{dif}/2$ is the phase imbalance. In a similar way, it can be shown that the quadrature-phase component of the synthesizer output can be expressed as

$$\begin{aligned} a_Q &= a_{com}(1-\epsilon) \\ \theta_Q &= \theta_{com} - \theta\,. \end{aligned} \tag{9}$$

By doing so, the down-conversion process as shown in Fig. 3 can be viewed as first performing a mixing the RF signal $V_{RF}(t)$ with an ideal LO. Afterwards, I-path and Q-path signals are cross-coupled according to the phase imbalance θ and then weighted by corresponding gain mismatch such that the input signals $V_{I,I}(t)$ and $V_{I,Q}(t)$ to the complex filter can be expressed as

$$\begin{aligned} V_{I,I}(t) &= V_{RF}(t) a_I \cos(\omega_{LO}t + \theta_I) \\ &= V_{RF}(t)(1+\epsilon) a_{com}\Big[\cos(\omega_{LO}t + \theta_{com})\cos\theta \\ &\quad - \sin(\omega_{LO}t + \theta_{com})\sin\theta\Big] \\ &= (1+\epsilon)\big(V_{X,I}(t)\cos\theta + V_{X,Q}(t)\sin\theta\big) \\ V_{I,Q}(t) &= (1-\epsilon)\big(V_{X,Q}(t)\cos\theta + V_{X,I}(t)\sin\theta\big)\,. \end{aligned} \tag{10}$$

where $V_{X,I}(t)$ and $V_{X,Q}(t)$ are the equivalent IF representation of RF signal.

MODELING OF COMPLEX FILTERS MISMATCH

In order to suppress the image signal, a complex bandpass filter after quadrature mixing is usually adopted in a low-IF receiver to pass the desired signal while attenuating the image signal. A complex filter can be designed by translating a lowpass transfer function into a complex bandpass one of which the asymmetric frequency response is used to differentiate the signal and the image. In general, complex filters take in-phase and quadrature phase signals as its inputs and generate two outputs followed by two analog to digital converters for digitalization. The two paths of digitized signals can be further processed by digital complex filters for a better image suppression; nevertheless, the trade-off for greater image rejection is the higher hardware cost. For commercial products, the requirement of interference

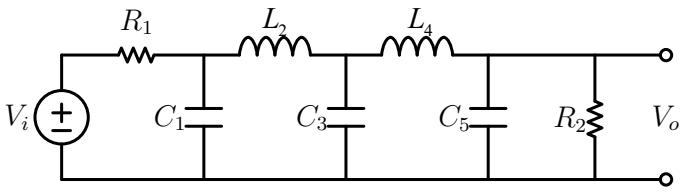

Fig. 5. Prototype of a LC-ladder lowpass filter.

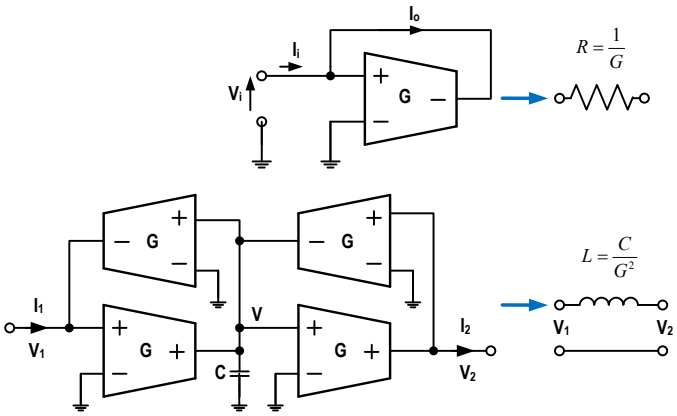

Fig. 6. Gm-C implementations for resistors and inductors.

rejection is not as stringent as for military usage. Therefore, we will hereafter assume only one ADC is utilized for digitizing analog samples, and analyze the tolerant imbalance between I/Q mixers and mismatch of complex filters for adequate image rejection.

The role of a complex BPF can be visualized by an example depicted in Fig. 4 where the desired signal is located at $\pm f_{RF}$ and the image is located at $\pm f_{IMG} = \pm|f_{LO} - f_{IF}|$. It is worth noting that for GPS/Galileo system, unlike the given example, the power spectrum density of the signal is far beneath the noise density and is not perceivable by a spectrum analyzer. For simplicity, both down-conversion mixers are assumed to be ideal, i.e., they perfectly perform frequency translation, shifting the received spectrum by an amount of $-f_{LO}$. After mixing, the desired signal is moved to f_{IF} while the unwanted image is located at $-f_{IF}$ plus some high frequency terms which can be simply filtered out. For a conventional real BPF with symmetric response, it will have equal gain for both the signal and the image; therefore, the image power will definitely degrades the reception performance. In contrast, as shown in Fig. 4(b), the complex filter with an asymmetric response is able to pass the signal and abate the image simultaneously, improving the receiver sensitivity. After filtering, the real part output of the complex filter is taken by one ADC, imposing the residual image onto the signal as in Fig. 4(d), however, if the complex filter is designed carefully, the residual image power is negligible.

For implementation of the complex filter, a Gm-C based lowpass filter [5], [6] originated from a LC-ladder prototype is used as a starting point and the response shifting in frequency domain is achieved by cross coupling transconductors between

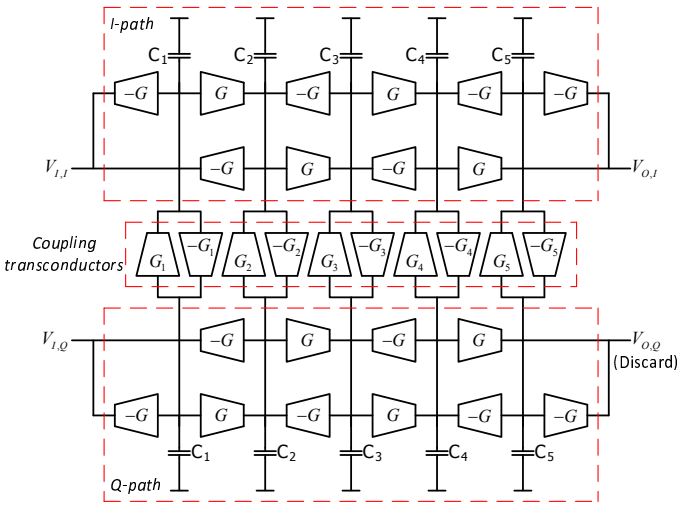

Fig. 7. Complete structure for a Gm-C implementation of the complex BPF.

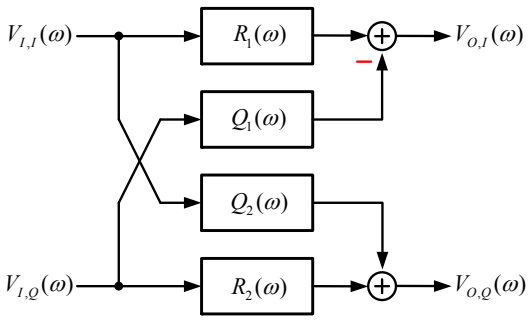

Fig. 8. Decompose a complex transfer function to four real transfer functions.

the I/Q paths. Consider a typical LC-ladder LPF shown in Fig. 5 as an example, those component values can be easily calculated [7] once the filter order and bandwidth are determined. Because the resistors and inductors are disadvantageous for integration, Gm-C implementations which use only transconductors and capacitors provide a better solution. The transformation formula is given in Fig. 6.

After replacement for the resistors and inductors in both I-path and Q-path, we will have two LPFs that have exactly the same response as their LC-ladder equivalence given that all components are ideal. The complex response can be obtained by inserting those transconductors (G_i) between I-path and Q-path as shown in the Fig. 7. The amount of shifting is also controlled by those transconductance as

$$\frac{G_i}{C_i} = \omega_{IF}, \quad \text{for } i = 1, \ldots, 5\,. \tag{11}$$

Undoubtedly, if all of the filter building components—transconductors and capacitors are perfect, the corresponding complex transfer function will be ideal as well. However, due to processing variations and layout imperfectness, those transconductance and capacitance will deviate from their designed values such that the image rejection ratio (IRR) will drop according to the level of inaccuracy of these components.

TABLE I
DESIGN VALUES OF FILTER PARAMETERS

Butterworth Order	C_1	C_2	C_3	C_4	C_5	Butterworth Order	C_1	C_2	C_3
5	1.92 pF	5.03 pF	6.22 pF	5.03 pF	1.92 pF	3	3.11 pF	6.22 pF	3.11 pF
G	G_1	G_2	G_3	G_4	G_5	G	G_1	G_2	G_3
40 μs	49.42 μS	129.37 μS	159.92 μS	129.37 μS	49.42 μS	40 μs	79.94 μS	159.87 μS	79.94 μS
Chebyshev (0.1 dB ripple) Order	C_1	C_2	C_3	C_4	C_5	Chebyshev (0.1 dB ripple) Order	C_1	C_2	C_3
5	3.58 pF	4.28 pF	6.16 pF	4.28 pF	3.58 pF	3	3.22 pF	3.58 pF	3.22 pF
G	G_1	G_2	G_3	G_4	G_5	G	G_1	G_2	G_3
40 μs	91.96 μS	109.95 μS	158.36 μS	109.95 μS	91.96 μS	40 μs	82.84 μS	92.14 μS	82.84 μS

Although using different type or order of filters will have different level of attenuation, the components mismatch will degrade the IRR performance no matter what kind of filters are used. As a result, the distorted response due to components mismatch needs careful consideration before actual implementation.

According to Fig. 8, it can be shown that the transfer function of a complex filter can be realized by four real transfer functions and the complex filter output is given by [8], [9]

$$V_{O,C}(\omega) = H_S(\omega)V_{I,C}(\omega) + H_M(\omega)V_{I,D}(\omega)\,, \quad (12)$$

where $V_{O,C}(\omega)$ is the frequency response of

$$V_{O,C}(t) = V_{O,I}(t) + jV_{O,Q}(t)\,, \quad (13)$$

and $V_{I,C}(\omega)$ and $V_{I,D}(\omega)$ is the frequency response of

$$V_{I,C}(t) = V_{I,I}(t) + jV_{I,Q}(t)\,, \quad (14)$$

and

$$V_{I,D}(t) = V_{I,I}(t) - jV_{I,Q}(t)\,, \quad (15)$$

respectively. As shown above, $V_{I,C}(t)$ and $V_{I,D}(t)$ are complex conjugate pair. That is, if $V_{I,C}(t)$ is regarded as the equivalent representation of the desired signal at the IF, $V_{I,D}(t)$ is the mirror image of it. Besides, $H_S(\omega)$ is the signal transfer function of the complex filter and can be expressed as

$$H_S(\omega) = \frac{\big(R_1(\omega) + R_2(\omega)\big) + j\big(Q_1(\omega) + Q_2(\omega)\big)}{2}\,,$$

and $H_M(\omega)$ is the mismatch transfer function of the complex filter and is derived as

$$H_M(\omega) = \frac{\big(R_1(\omega) - R_2(\omega)\big) + j\big(Q_2(\omega) - Q_1(\omega)\big)}{2}\,.$$

Ideally, given no mismatch of components, $R_1(\omega)$ will equal to $R_2(\omega)$ and $Q_1(\omega)$ will equal to $Q_2(\omega)$ as well such that $H_M(\omega)$ will be zero and $H_S(\omega)$ will be identical to its lowpass counterpart except the central frequency is now situated at ω_{IF} rather than at D.C.

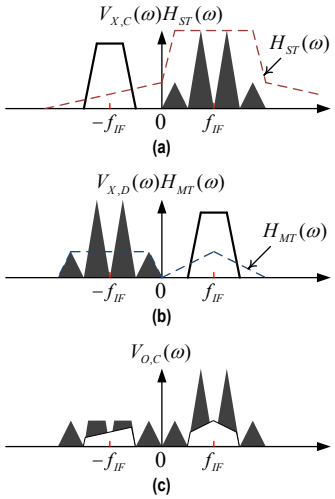

Fig. 9. An example of overall signal and mismatch transfer functions.

From (10) and (12), the effects of I/Q imbalance can be included and the complex filter output can be reformulated as

$$V_{O,C}(\omega) = H_{ST}(\omega)V_{X,C}(\omega) + H_{MT}(\omega)V_{X,D}(\omega)\,, \quad (16)$$

where

$$\begin{aligned} H_{ST}(\omega) = {} & H_S(\omega)(\cos\theta - j\epsilon\sin\theta) \\ & + H_M(\omega)(\epsilon\cos\theta - j\sin\theta)\,, \end{aligned} \quad (17)$$

is the overall signal transfer function and

$$\begin{aligned} H_{MT}(\omega) = {} & H_S(\omega)(\epsilon\cos\theta + j\sin\theta) \\ & + H_M(\omega)(\cos\theta + j\epsilon\sin\theta)\,. \end{aligned} \quad (18)$$

is the overall mismatch transfer function. Analogous to (14) and (15), $V_{X,C}(\omega)$ and $V_{X,D}(\omega)$ is the frequency response of

$$V_{X,C}(t) = V_{X,I}(t) + jV_{X,Q}(t)\,, \quad (19)$$

and

$$V_{X,D}(t) = V_{X,I}(t) - jV_{X,Q}(t)\,, \quad (20)$$

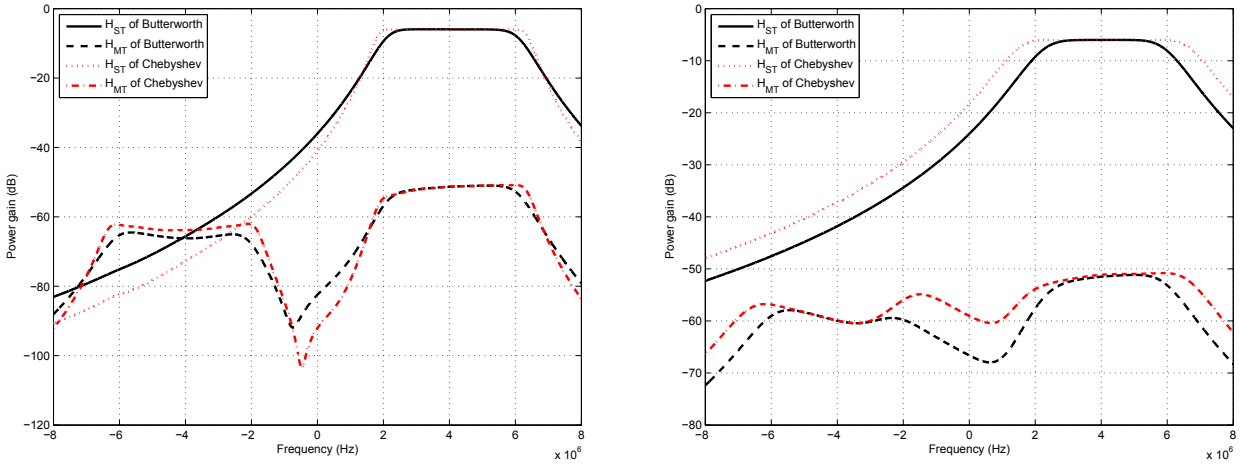

(a) 5th-order Butterworth and Chebyshev complex filters.

(b) 3rd-order Butterworth and Chebyshev complex filters.

Fig. 10. $H_{ST}(\omega)$ and $H_{MT}(\omega)$ of Butterworth and 0.1 dB ripple Chebyshev complex filters with the maximum of 1% independent components mismatch of filters.

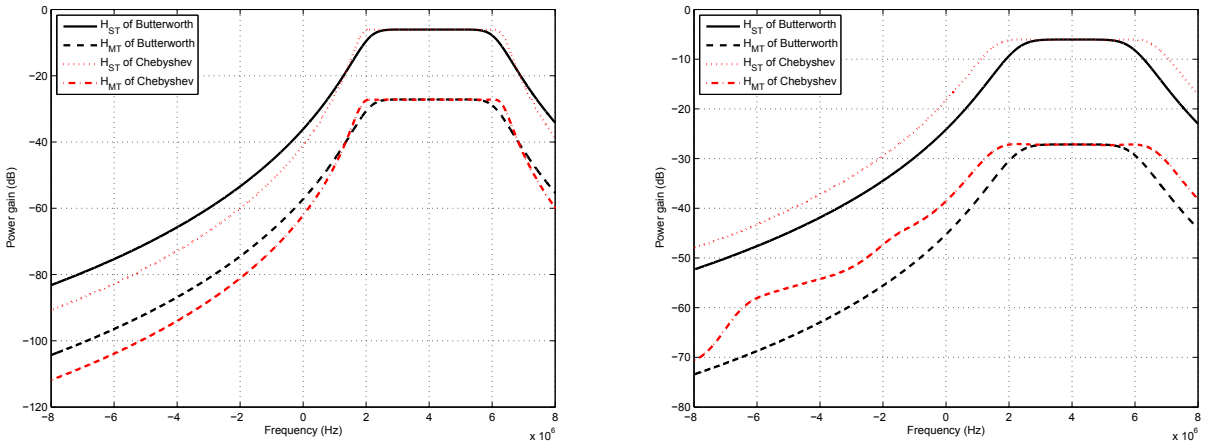

(a) 5th-order Butterworth and Chebyshev complex filters.

(b) 3rd-order Butterworth and Chebyshev complex filters.

Fig. 11. $H_{ST}(\omega)$ and $H_{MT}(\omega)$ of Butterworth and 0.1 dB ripple Chebyshev complex filters with 5% amplitude and 5° phase imbalance of mixers.

respectively. A typical spectral representation for $H_{ST}(\omega)$ and $H_{MT}(\omega)$ is given in Fig. 9. It is obvious that $V_{X,C}(\omega)$ and $V_{X,D}(\omega)$ mirror with respect to D.C., and $H_{ST}(\omega)$ is responsible for retaining the signal portion of positive frequency while image is rejected according to the stop-band attenuation of the filter. Including the nonideal effects of I/Q mixers, $H_{MT}(\omega)$ let unwanted image of both positive and negative frequency components into reception. Although the negative frequency components of $V_{X,C}(\omega)H_{ST}(\omega)$ and $V_{X,D}(\omega)H_{MT}(\omega)$ could be further mitigated by a digital complex filter in baseband, if the complex filter output is sampled by two distinct ADCs for both I/Q paths, the positive frequency component of $V_{X,D}(\omega)H_{MT}(\omega)$, however, is unable to be separated and eliminated easily, particularly if the image signal is not a prior information to the receiver.

From Fig. 9, there are three different sources of interference, the first one is the image attenuated by the negative frequency of $H_{ST}(\omega)$, the second is the signal attenuated by the negative frequency of $H_{MT}(\omega)$, both interference are out-of-band, and the third is the image attenuated by the positive frequency of $H_{ST}(\omega)$ which is the in-band interference. Accordingly, the receiver performance in terms of the carrier to noise ratio (C/N) can now link with the IRR as

$$\frac{C}{N} = \frac{C}{N_0 + N_I} = \frac{C}{N_0} \cdot \frac{1}{1 + \mathrm{IRR}^{-1}}, \tag{21}$$

where N_I are three additional interference power, N_0 is the ubiquitous AWGN, and IRR is defined as

$$\begin{aligned} \mathrm{IRR} &\triangleq \frac{N_0}{N_I} \\ &= \frac{|H_{ST}(\omega_{IF})|^2}{|H_{ST}(-\omega_{IF})|^2 + |H_{MT}(-\omega_{IF})|^2 + |H_{MT}(\omega_{IF})|^2}. \end{aligned} \tag{22}$$

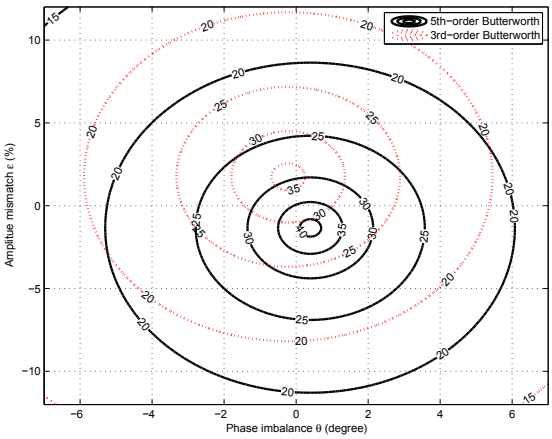

(a) Butterworth complex filters.

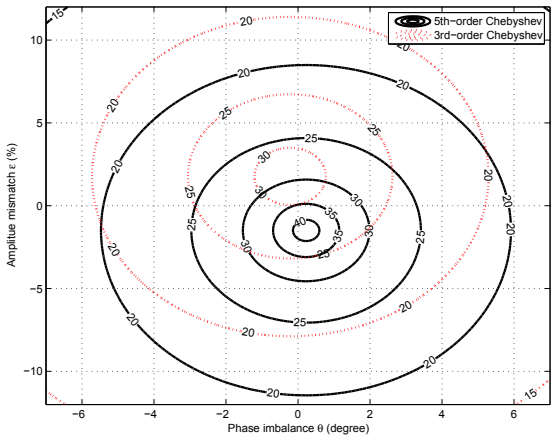

(b) Chebyshev complex filters.

Fig. 12. IRR (dB) contour for Butterworth and 0.1 dB ripple Chebyshev complex filters with the maximum of 1% independent components mismatch of filters.

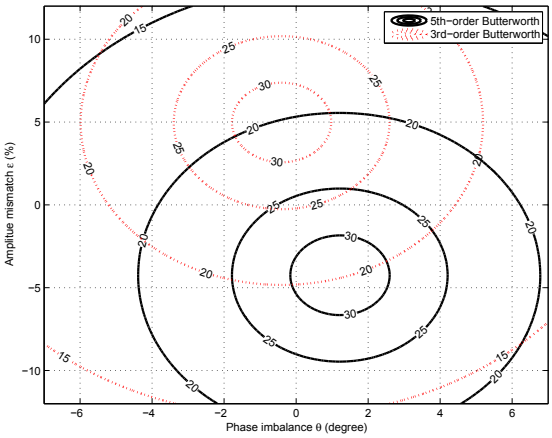

(a) Butterworth complex filters.

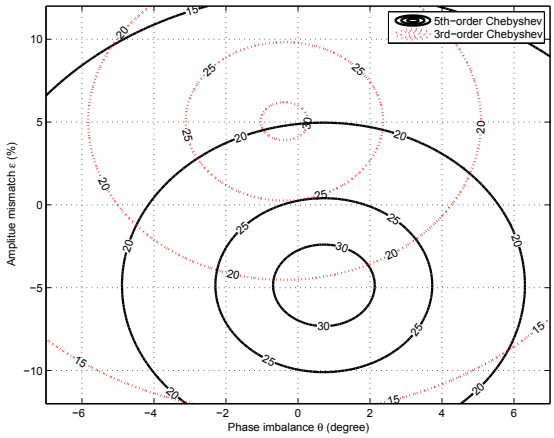

(b) Chebyshev complex filters.

Fig. 13. IRR (dB) contour for Butterworth and 0.1 dB ripple Chebyshev complex filters with the maximum of 3%independent components mismatch of filters.

SIMULATION RESULTS

For demonstration the usefulness of the proposed evaluating method, the single stage down-conversion low-IF prototype GPS/Galileo receiver is modeled with the IF located at 4.092 MHz. The receiver's analog front-end contains a passive antenna, two quadrature mixers, a Gm-C type complex filter and one ADC. Two different types of response—Butterworth and Chebyshev filters of both 5th- and 3rd-order are considered in this work for comparing their performances of IRR. We targeted for an IRR of 25 dB since it will introduce approximately about 0.01 dB of C/N loss [10] that is usually acceptable in most cases. According to the Butterworth and Chebyshev prototype of LC-ladder filters, the design parameters of filters after Gm-C transformed are summarized in Table I where the values of G_i are chosen for the purpose of having a frequency shift of 4.092 MHz. CAD tool of Agilent Advanced Design System (ADS) is adopted to build the testbed and Monte Carlo simulation is used to verify the correctness of predicted IRR.

In order to evaluate the IRR performance based on (22), both transfer functions of $H_{ST}(\omega)$ and $H_{MT}(\omega)$ are needed. From (16), $H_{ST}(\omega)$ will be the transfer function of $\frac{V_{O,C}(\omega)}{V_{X,C}(\omega)}$ if the mirror spectrum $V_{X,D}(\omega)$ is zero, so will its time domain representation given by (20) be, whose trivial solution can be found by setting $V_{X,I}(t) = 1$ and $V_{X,Q}(t) = -j$. That is,

$$H_{ST}(\omega) = \left.\frac{V_{O,C}(\omega)}{V_{X,C}(\omega)}\right|_{V_{X,I}(t)=1, V_{X,Q}(t)=-j}, \qquad (23)$$

and $H_{MT}(\omega)$ can be obtained in a similar way except alternating the polarity of $V_{X,Q}(t)$ as

$$H_{MT}(\omega) = \left.\frac{V_{O,C}(\omega)}{V_{X,D}(\omega)}\right|_{V_{X,I}(t)=1, V_{X,Q}(t)=j}. \qquad (24)$$

From previous discussion, the effects of mismatch transfer function $H_M(\omega)$ will be negligible if the complex filter is perfectly matched. As a result, we consider the filter components mismatch errors of maximum of 1% deviation from

their nominal values, but the amplitude and phase imbalance of mixers are kept ideal first, the worst case scenario out of 50,000 independent runs are selected and plotted in Fig. 10. Because the mixers are ideal, from (17) and (18), we have $H_{ST}(\omega) = H_S(\omega)$ and $H_{MT}(\omega) = H_M(\omega)$. According to the simulation results, the signal transfer function $H_S(\omega)$ is hardly affected by the mismatch, but the imbalance between I-path and Q-path components do cause a large portion of interference power on the reception which is predicted by $H_M(\omega)$.

As for the effects of mixers imbalance, filter mismatch is temporarily ignored and 5% of amplitude imbalance and 5° phase imbalance are assumed. From both Fig. 11(a) and Fig. 11(b), we can notice that $H_{ST}(\omega)$ and $H_{MT}(\omega)$ have similar response except for a different gain. That is also expectable because the mismatch transfer function $H_M(\omega)$ is almost zero hence both $H_{ST}(\omega)$ and $H_{ST}(\omega)$ are dominated by the signal transfer function $H_S(\omega)$ and are weighted in accordance with ϵ and θ. Unlike the case of filter mismatch, the overall mismatch transfer function $H_{MT}(\omega)$ will have a higher gain within the signal band, that is, the interference will directly intermix with the desired signal and cannot be separated out in the following baseband unless the interference is estimated and advanced DSP techniques are used to cancel the interfering power.

In Fig. 12 and Fig. 13 where the maximum independent errors of filter components are 1% and 3% respectively, the worst case simulation results are given for both Butterworth and Chebyshev filters. For all of the sub-figures, x-axis is the phase imbalance (θ) in degree and y-axis is the relative percentage of amplitude mismatch (ϵ). Because the filters are nonideal, the centre of circles of these contour plots do not locate on the point where both amplitude and phase mismatch are zero. According to the simulation results summarized in Table II, for a targeted IRR of 25 dB, both types of filters have comparable tolerance for mixer imbalance, and because of the better image rejection provided by higher order filters, they possess relatively higher tolerance of mixers imbalance comparing to their lower order counterparts. However, in a hostile scenario where deliberate interference is encountered, the required IRR needs to be increased in order to maintain the same signal quality. In such situation, the tolerance region for lower order filters is shrunk drastically that is also revealed from the simulation results.

TABLE II
TOLERENCE OF MIXER IMBALANCE

	5th-order Butterworth	3rd-order Butterworth	5th-order Chebyshev	3rd-order Chebyshev
	1% independent errors of filter components			
$\lvert\epsilon_{\max}\rvert$ [%]	4.2	3.8	4.2	3.2
$\lvert\theta_{\max}\rvert$ [°]	2.8	2.9	3.0	2.7
	3% independent errors of filter components			
$\lvert\epsilon_{\max}\rvert$ [%]	1.0	0.2	0.4	n/a
$\lvert\theta_{\max}\rvert$ [°]	1.8	2.6	2.3	n/a

Based on 25 dB IRR requirement.

CONCLUSIONS

Nowadays a low-IF architecture draws lots of attention for GPS/Galileo receiver not only for its cheaper implementation cost but also for its promised performance. However, good performance can be achieved only when the image problem is carefully controlled and mitigated. Thus it is urged for comprehensively modeling both quadrature mixers and the following complex filters that are main contribution to imperfect IRR in the front-end. In this work, based on the approach to precisely model both the I/Q imbalance of mixers and components mismatch in complex filters, the linkage between IRR and C/N performance can further provide a better understanding the effects of image on system performance and shed some light on the requirement of IRR for a GPS/Galileo system designer.

ACKNOWLEDGMENT

The authors would like to thank the support (in part) by MediaTek Inc.

REFERENCES

[1] A. Schmid and et al., "A combined Galileo/GPS receiver architecture for consumer market applications," *NAVITEC 2004, ESA ESTEC*, Nordwijk, Netherlands, 8–10 December, 2004.

[2] R. Berenguer, J. Mendizabal, U. Alvarado, D. Valderas, and A. García-Alonso, "A low power low noise figure GPS/Galileo front-end for handheld applicatoin in a 0.35μm SiGe process," *Radio Frequency Integrated Circuits (RFIC) Symposium*, 11–13 June, 2006.

[3] D. K. Shaeffer and et al., "A 115-mW, 0.5-μm CMOS GPS receiver with wide dynamic-range active filters," *IEEE J. Solid-State Circuits*, vol. 33, no. 12, pp. 2219–2231, December 1998.

[4] J. W. Betz, "The offset carrier modulation for GPS modernization, *Proc. of ION National Technical Meeting*, pp. 639–648, 1999.

[5] F. Behbahani and et al., "A fully integrated low-IF CMOS GPS radio with on-chip analog image rejection," *IEEE J. Solid-State Circuits*, vol. 37, no. 12, pp. 1721–1727, December 2002.

[6] B. Guthrie, J. Hughes, T. Sayers, and A. Spencer, "A CMOS gyrator low-IF filter for a dual-mode Bluetooth/ZigBee transceiver," *IEEE J. Solid-State Circuits*, vol. 40, no. 9, pp. 1872–1879, September 2005.

[7] R. Schaumann and M. E. van Valkenburg, *Design of Analog Filters*, New York, Oxford Univ. Press, 2001.

[8] J. Mahattanakul, "The effect of mismatch in $Gm-C$ polyphase filters," *IEEE Trans. Circuits Syst. II, Exp. Briefs*, vol. 52, no. 7, pp. 410–414, July 2005.

[9] J. Mahattanakul, "The effect of I/Q imbalance and complex filter component mismatch in low-IF receivers," *IEEE Trans. Circuits Syst. I, Reg. Papers*, vol. 53, no. 2, pp. 247–253, February 2006.

[10] J. Ko, J. Kim, S. Cho, and K. Lee, "A 19-mW 2.6-mm^2 L1/L2 dual-band CMOS GPS receiver," *IEEE J. Solid-State Circuits*, vol. 40, no. 7, pp. 1414–1425, July 2005.